Biogeosciences Discuss., 7, 6675–6704, 2010
www.biogeosciences-discuss.net/7/6675/2010/
doi:10.5194/bgd-7-6675-2010

Biogeosciences Discussions

Synoptic relationships quantified between surface Chlorophyll-*a* and diagnostic pigments specific to phytoplankton functional types

T. Hirata[1,2,*,], N. J. Hardman-Mountford[1,2], R. J. W. Brewin[3], J. Aiken[1], R. Barlow[4], K. Suzuki[5], T. Isada[6], E. Howell[7], T. Hashioka[8,9], M. Noguchi-Aita[6,9], and Y. Yamanaka[5,8,9]**

[1]Plymouth Marine Laboratory (PML), Plymouth, UK
[2]National Centre for Earth Observation (NCEO), UK
[3]School of Marine Science and Engineering, University of Plymouth, Plymouth, UK
[4]Marine and Coastal Management, Cape Town, South Africa
[5]Faculty of Environmental Earth Science, Hokkaido University, Sapporo, Japan
[6]Faculty of Fisheries Sciences, Hokkaido University, Hakodate, Japan
[7]Pacific Island Fisheries Science Centre, National Oceanic and Atmospheric Administration (NOAA), Hawaii, USA

[8]Core Research for Evolution Science and Technology (CREST), Japan Science Technology Agency, Japan
[9]Research Institute for Global Change, Japan Agency for Marine-Earth Science and Technology (JAMSTEC), Yokohama, Japan
[*]now at: Faculty of Environmental Earth Science, Hokkaido University, Japan
[**]now at: Core Research for Evolution Science and Technology (CREST), Japan Science Technology Agency, Japan

Received: 29 July 2010 – Accepted: 26 August 2010 – Published: 1 September 2010

Correspondence to: T. Hirata (tahi@ees.hokudai.ac.jp)

Published by Copernicus Publications on behalf of the European Geosciences Union.

BGD
7, 6675–6704, 2010

Abstract

Error-quantified, synoptic-scale relationships between chlorophyll-*a* (Chl*a*) and phytoplankton pigment groups at the sea surface are presented. A total of nine pigment groups were considered to represent nine phytoplankton functional types (PFTs) including microplankton, nanoplankton, picoplankton, diatoms, dinoflagellates, green algae, picoeukaryotes, prokaryotes and *Prochlorococcus* sp. The observed relationships between Chl*a* and pigment groups were well-defined at the global scale to show that Chl*a* can be used as an index of not only phytoplankton abundance but also community structure; large (micro) phytoplankton monotonically increase as Chl*a* increases, whereas the small (pico) phytoplankton community generally decreases. Within these relationships, we also found non-monotonic variations with Chl*a* for certain pico-plankton (pico-eukaryotes, Prokaryotes and *Prochlorococcus* sp.) and for Green Algae and nano-sized phytoplankton. The relationships were quantified with a least-square fitting approach in order to estimate the PFTs from Chl*a* alone. The estimated uncertainty of the relationships quantified depends on both phytoplankton types and Chl*a* concentration. Maximum uncertainty over all groups (34.7% Chl*a*) was found from diatom at approximately Chl*a* = 1.07 mg m^{-3}. However, the mean uncertainty of the relationships over all groups was 5.8 [% Chl*a*] over the entire Chl*a* range observed (0.02 < Chl*a* < 6.84 mg m^{-3}). The relationships were applied to SeaWiFS satellite Chl*a* data from 1998 to 2009 to show the global climatological fields of the surface distribution of PFTs. Results show that microplankton are present in the mid and high latitudes, constituting ~ 9.0 [% Chl*a*] of the phytoplankton community at the global surface, in which diatoms explain ~ 6.0 [% Chl*a*]. Nanoplankton are ubiquious throught much of the global surface oceans except subtropical gyres, acting as a background population, constituting ~ 44.2 [% Chl*a*]. Picoplankton are mostly limited in subtropical gyres, constituting ~ 46.8 [% Chl*a*] globally, in which prokaryotes are the major species explaining 32.3 [% Chl*a*] (*prochlorococcus* sp. explaining 21.5 [% Chl*a*]), while pico-eukaryotes are

BGD

7, 6675–6704, 2010

notably abundant in the Southern Pacific explaining ~ 14.5 [% Chl*a*]. These results may be used to constrain or validate global marine ecosystem models.

1 Introduction

Phytoplankton play numerous roles in ocean biogeochemical cycling: CO_2 is utilised to form organic matters such as carbohydrates in photosynthetic processes and is then released through respiration; macro- and micronutrients are assimilated by phytoplankton for their metabolisms. While these examples are common to all phytoplankton, some species require specific chemical compounds for their distinct physiological processes, thereby fulfilling a range of different functional roles in the ocean biogeochemical cycles: Si is utilised by diatoms, Ca by coccolithophores and N_2 by some cyanobacteria (e.g. *Trichodesmium*). Some phytoplankton (e.g. dinoflagellates, prymnesiophytes) appear responsible for enhanced DMSp production in the ocean, contributing to an exchange of S between the ocean and atmosphere (see Nair et al., 2008 for review). These functional differences have led to phytoplankton being classed according to their functional types.

In order to quantify the contributions of these phytoplankton functional types (PFTs) to biogeochemical cycling on a global scale, it is first important to understand their spatiotemporal variability throughout the oceans. Ocean biogeochemistry and ecosystem models, such as NEMURO (Kishi et al., 2007; Aita et al., 2007; Hashioka and Yamanaka, 2007), ERSEM (Blackford et al., 2004; Petihakis et al., 2005), PlankTOM-5 and -10 (Le Quéré et al., 2005; Le Quéré and Pesant, 2009) and NOMB (e.g. Gregg et al., 2003, 2007), can be used to investigate the processes responsible for spatial and temporal variability of phytoplankton populations at large scales and provide some potential for forecasting future ocean states. The populations within these models are generally based on biogeochemical function (usually linked to size), rather than explicit taxonomy. Validation of these models is essential, which is cumbersome when large

BGD
7, 6675–6704, 2010

spatial and temporal scales are concerned (Allen et al., 2010), so requires a globally consistent approach based on a functional classification of marine phytoplankton groups.

In general, the agreement between functional- and taxonomic- or size-based classifications, while far from universal, is adequate for comparisons to be undertaken with current model estimates. The close similarity between the functional classification of Le Quéré et al. (2005) and size structure or taxonomic groupings is shown in Table 1. On the other hand, direct estimation of phytoplankton community structure at basin to global scales is non-trivial. Traditional microscopic observations, flow cytometry, pigment and DNA analyses have all been used to classify phytoplankton community structure in situ. Pigment analysis by High Performance Liquid Chromatography (HPLC) has become increasingly popular in oceanography because of the relatively large number of samples that can be collected and analysed rapidly, categorizing the phytoplankton community (at least according to broad classes based on size or taxonomy) much faster than with traditional microscopy. Even so, spatial and temporal coverage is inevitably limited by the mismatch in scales between in situ observational capabilities and the vast size of the oceans.

Since the launch of the ocean colour sensor, satellites have been able to provide a continuous record of multi-spectral optical observations of the ocean surface, that at certain wavelengths correspond strongly to concentrations of the ubiquitous photosynthetic pigment, chlorophyll-*a* (Chl*a*). From this proxy of phytoplankton biomass, variations in oceanic phytoplankton populations and global marine primary production have been investigated (e.g. Longhurst et al., 1995; Behrenfeld and Falkowski, 1997; Behrenfeld et al., 2006; Polovina et al., 2008). More recently, this technology has revealed the capability for more in depth investigation of phytoplankton community structure by means of PFTs or size classes (e.g. Sathyendranath et al., 2004; Alvain et al., 2005, 2008 ; Ciotti et al., 2002; Devered et al., 2006; Uitz et al., 2006; Aiken et al., 2007, 2009; Hirata et al., 2008; Raitsos et al., 2008; Brewin et al., 2010), allowing the extrapolation of in situ PFT descriptions to larger spatial scales with better

BGD
7, 6675–6704, 2010

temporal resolution, thus providing a method to more adequately constrain and validate biogeochemical and ecosystem models.

The current suite of satellite PFT algorithms are derived from either (1) the "dominance" of specific PFTs or size classes without estimation of their fractional contributions to the overall phytoplankton community (Sathyendranath et al., 2004; Alvain et al., 2004, 2008; Hirata et al., 2008; Raitsos et al., 2008), or (2) a limited number of phytoplankton size classes such as micro-, nano-, and picoplankton (Devred et al., 2006; Uitz et al., 2006; Brewin et al., 2010), for which the fractional contribution is in some cases estimated. Our scope in this paper is to bridge the gap between these approaches by estimating the fractional contribution of an increased number of PFTs, partitioned within 3 size classes where appropriate. We use global relationships from in situ data to derive climatological distributions of PFTs from satellite Chl*a* measurements. Relationships between phytoplankton Chl*a* concentrations and the phytoplankton functional types determined from their biomarker pigments are quantified from a global in situ data, and uncertainty is presented on these relationships. The quantified relationships are also applied to monthly 1 satellite observations of Chl*a* fields to estimate the synoptic distributions of PFTs in the world's oceans.

2 Data

2.1 In situ pigment data

Phytoplankton pigments derived from High Performance Liquid Chromatography (HPLC) were obtained from various sources, including the Atlantic Meridional Transect programme (AMT) by the Natural Environmental Research Council (NERC, UK), the BEAGLE cruise by Japan Agency for Marine-Earth Science and TEChnology (JAMSTEC, Japan), the SeaWiFS Bio-optical archive and Storage System (SeaBASS) by National Aeronautics and Space Administration (NASA, USA), the NASA bio-Optical Marine Algorithm Dataset (NOMAD), the SEEDS II experiment by the University of

BGD
7, 6675–6704, 2010

Tokyo (Japan), A-line stations by Fisheries Research Agency (FRA, Japan), and the Oshoro-Maru cruise by Hokkaido University (HU, Japan) (Fig. 1). Only surface data (< 10 m) were used ($N = 5886$), consistent with the application of this study to satellite ocean colour observations. The data were quality controlled in the following way: individual pigment data were visually checked and data of clear low-quality (e.g. continuously repeated value over several stations within a cruise, typically low values, suspected as outside the detection limits of an instrument) were removed. Further outliers were determined from the regression of accessory pigments against Chl*a* concentration, excluding values beyond the 95% confidence interval of the regression (Aiken et al., 2009). The data were then sorted by numerical value of Chl*a* and smoothed with a 5 point running mean low-pass filter to improve the signal to noise ratio (Hirata et al., 2008; Brewin et al., 2010). Among the quality controlled data, 70% of them were used for algorithm development whereas 30% were reserved for validation. The validation data were constructed in such a way that 30% of each sub-dataset (i.e. each cruise or dataset mentioned earlier) was sub-sampled randomly and collected, using a random number generator, to ensure that each sub-dataset evenly contributes to the validation dataset.

2.2 Satellite ocean colour data

SeaWiFS 9km Level-3 monthly composites of Chl*a* data for the period 1998–2009 were obtained from NASA Goddard Space Flight Centre using the latest 2009 reprocessing which has resulted in improved atmospheric and radiometric corrections, more comprehensive vicarious calibration and corrections to instrument calibration drift over the time series. Validation results show substantially improved agreement with in situ measurements in turbid and highly productive waters (see http://oceancolor.gsfc.nasa.gov/REPROCESSING/R2009/ and linked forum topics for further details). In order to focus on oceanic waters, coastal and shelf waters (< 200 m) were masked out in the SeaWiFS Chl*a* data, using the ETOPO5 bathymetry obtained from National Geophysical Data Centre.

BGD
7, 6675–6704, 2010

3 Methods

Diagnostic Pigment Analysis (DPA) is applied to classify phytoplankton types from HPLC pigment data (Vidussi et al., 2001). DPA defines a suite of Diagnostic Pigments (DP) for specific PFTs that can be quantified relative to the sum of all DP concentrations (i.e. DP/ΣDP) to estimate the relative abundance of a specific PFT (Table 1). The DPA procedure, originally proposed by Vidussi et al. (2001), was subsequently refined by Uitz et al. (2006) to scale ΣDP to Chl*a*, permitting the application of DPA-based approaches to satellite-derived Chl*a*. In addition, Hirata et al. (2008) used the refined DPA to separate pico-eukaryotes from nano-eukaryotes, and Brewin et al. (2010) developed a method to quantify the relationship, which is used in the present work. Here, DPA is further refined to account for ambiguity of the fucoxanthin (Fuco) signal. Fuco is defined as a DP for Diatoms by Vidussi et al. (2001). However, Fuco is also a precursor pigment of 19′-Hexanoyloxyfucoxanthin (Hex), the DP for prymnesiophytes, and can co-occur in this group. Fuco is also contained in the other heterokonts (e.g. chrysophytes, bolidophytes) and dinoflagellates (Wright and Jeffrey, 2006). Thus, diatoms could be overestimated in DPA. Hirata et al. (2008) found a non-negligible proportion of Fuco within the oligotrophic gyres of the subtropical Atlantic, where small prokaryotes (predominantly *Prochlorococcus* sp. and *Synecococcus* sp.) and pico-eukaryotes (which can partly belong to the prymnesiophytes so may also contain Hex) usually dominate the phytoplankton community (Zubukov et al., 1998; Tarran et al., 2006). In these oligotrophic waters, Chl*a* is low ($< 0.25\,mg\,m^{-3}$, Aiken et al., 2009), therefore, it is more reasonable to assume that the background level of Fuco detected results from smaller prymnesiophytes rather than diatoms which are more prevalent in eutrophic waters. Therefore, we calculated the baseline of Fuco/Hex ratio, (Fuco/Hex)baseline, using Fuco and Hex at Chl*a* range less than $0.25\,mg\,m^{-3}$ in the original data set (Fucooriginal and Hexoriginal, respectively). A proportion of Fuco as a diatom biomarker is corrected so that Fucocorrected = Fuco – (Fuco/Hex)baseline × Hexoriginal. The Fuco

BGD
7, 6675–6704, 2010

conversion is only significant in the lower Chl*a* range ($< 0.5\,mg\,m^{-3}$) and is negligible for higher Chl*a* values.

4 Results and discussion

4.1 Synoptic relationships between Chl*a* and phytoplankton functional types (PFTs)

Figure 2 shows the global relationships between Chl*a* and the fraction of DP associated with each PFT, derived from in situ HPLC. Well-defined, co-variability is found between Chl*a* and DP for each PFT. While Chl*a* is known as an index of phytoplankton biomass, the co-variability indicates that Chl*a* is also an index of phytoplankton community structure. For microplankton, the fractional contribution to Chl*a* (% Chl*a*) monotonically increases with increasing Chl*a* (Fig. 2a), whereas for picoplankton, this monotonically decreases with increasing Chl*a* (Fig. 2c). Micro- and picoplankton in our data fall in the ranges of 0–87 and 6–90 [% Chl*a*], respectively, showing a large variation in time or space. The relationship between Chl*a* and nanoplankton does not show the monotonic variations found in micro- and picoplankton (Fig. 2b). Rather % Chl*a* of nanoplankton increases as Chl*a* increases up to approximately $0.2\,mg\,m^{-3}$ but decreases as Chl*a* further increases, resulting in a broad maximum between $0.1–0.3\,mg\,m^{-3}$ approximately. Nanoplankton ranges from 7–72 [% Chl*a*], showing a smaller range of variation than that of micro- and picoplankton.

These size-class relationships (micro-, nano-, and picoplankton) are further decomposed into a range of PFTs. Microplankton (Fig. 2a) is subdivided into diatoms and dinoflagellates (Fig. 2d and g), and their abundance ratios vary against Chl*a* with a similar relationship to that of microplankton. Picoplankton is composed of pico-eukaryotes and prokaryotes (Fig.2f and h), the latter of which include *Prochlorococcus* sp. (Fig. 2i). Not all of the abundance ratios within the picoplankton community vary in a same fashion. The % Chl*a* of prokaryotes and *Prochlorococcus* sp. non-monotonically

BGD
7, 6675–6704, 2010

decreases with Chl*a* with a local maxima, which occurs at Chl*a* = 0.08 – 1.00 mg m^3 (Fig. 2h and i). Pico-eukaryotes also show a non-monotonic variation with Chl*a* but shows a local minima; % Chl*a* being higher for Chl*a* < 0.04 mg m^{-3}, then decreasing up to 0.09–0.10 mg m^{-3}, increasing slightly up to 0.80 mg Chl*a* m^{-3}, then decreasing gradually again above it. Pigment classification is unable to discriminate the size ranges of green algae (e.g. Suzuki et al., 2002) therefore it is not explicitly classified according to a specific size class here. The % Chl*a* of green algae shows a broad peak shifted to Chl*a* values between 0.5 and 0.9 mg m^{-3}.

The relationships between Chl*a* and % Chl*a* shown above can be quantified using the least square fit (thick solid lines in Fig. 2), enabling the estimation of % Chl*a* of each PFT from Chl*a* alone, hence from satellite-derived Chl*a* fields (O'Reilly et al., 1998). Table 2 summarizes the fitting formulae and associated coefficients to quantify the relationship between Chl*a* and % Chl*a* for each PFT. While the relationships between Chl*a* and % Chl*a* of Micro- and Picoplankton were represented using a classical logistic equation, the relationships in the other PFTs were not expressed by the equation. Thus, the use of the logistic growth model was only applicable to a limited number of phytoplankton (Micro, diatoms and Pico) in our data set.

Fitting functions other than those shown in Table 2, such as polynomials for example, could be used for fitting. However, they tend to over- or underestimate at lower and upper bounds of the Chl*a* range observed, without introducing a significant statistical improvement (hence, results not shown). When polynomial fitting is used to extrapolate outside the Chl*a* range in Fig. 2, which would be necessary for satellite data processing, they would introduce larger errors than those shown in Table 3. Hence, we did not employ polynomial fitting.

To maintain "mass balance", not all relationships are regressed. For example, % Chl*a* of nanoplankton is derived from 100 – % Chl*a* (microplankton) – % Chl*a* (picoplankton) so that micro-, nano- and picoplankton sum up to 100%. The nanoplankton relationship derived in this way (shown as a thin curve in Fig. 2b) still fits the observed data well, reflecting strength in the micro- and picoplankton fits. This subtraction could equally

BGD
7, 6675–6704, 2010

have been undertaken between micro- and nano-phytoplankton derived from regression, or similarly between nanoand pico-phytoplankton. However, the best statistical fit was found in our data set when % Chl*a* (nanoplankton) was not regressed. The method was also used to derive dinoflagellates within the micro-phytoplankton community and pico-eukaryotes within the pico-phytoplankton community.

Figure 3 shows the estimated uncertainties of the relationships between % Chl*a* and Chl*a*, defined here as the residual between in situ data and the least-square fit. The uncertainty varies according to both the PFT considered and the Chl*a* level. Maximum mean uncertainty (i.e. maximum Root Mean Square Error, RMSE), is 7.5 [% Chl*a*] for nanoplankton (Fig. 3h), while minimum is 2.3 [% Chl*a*] for dinoflagellates (Fig. 3g). The overall mean uncertainty is 5.8 [% Chl*a*] when all PFTs are considered (Table 3). The uncertainty is variable even within a specific PFT considered. For example, the local maximum of uncertainty is as high as 33.0 [% Chl*a*] at Chl*a* of 1.07 mg m^{-3} for microplankton (Fig. 3a; see also Table 3), and 34.7 [% Chl*a*] at 1.07 mg m^{-3} for diatoms (Fig. 3d). Thus the regressions obtained in Fig. 2 would represent synoptic relationships between Chl*a* and % Chl*a* of each PFT, and small scale variability of PFT, both in time and space, may not be represented in our proposed formulations.

4.2 Validation of the relationships between Chl*a* and PFTs

Figure 4 shows a graphical representation of validation results. The derived relationships generally perform well, which is confirmed by the statistical results shown in Table 4; the mean regression slopes are close to unity (0.951), the intercept close to zero (−0.785), high coefficient of determination ($r^2 = 0.601$) and small error (RMSE = 5.99 [%]). Detailed statistics show that the algorithm performance varis according to the the PFT of interest. While the picoplankton algorithm performed particularly well ($r^2 = 0.835$), the dinoflagellate algorithm did rather poorly ($r^2 = 0.089$) which resulted in the significant reduction of the mean r^2 (= 0.587) over all PFTs. Careful examination of dinoflagellates (Fig. 4g), microplankton (Fig. 4a) and diatoms (Fig. 4b) suggests that the estimation of large-cell phytoplankton are less accurate

BGD
7, 6675–6704, 2010

at < 9 [% Chl*a*] (Recall the uncertainties for these PFTs are 6.7, 6.6 and 2.3 % Chl*a*). Nanoplankton (Fig. 4b), Green Algae (Fig. 4e) and *Prochlorococcus* sp. (Fig. 4i) indicate artificial cut-offs at the higher end of the estimated % Chl*a*. This results from the fact that (1) the relationships between Chl*a* and % Chl*a* of PFTs are formulated by the least-square regression, so that a single value of Chl*a* returns a single value of % Chl*a* and (2) the functional forms of the relationships for these particular PFTs show a local maxima which is also the maximum over the given range of Chl*a*, thus does not allow to return % Chl*a* above the maximal value; for example, see Fig. 2b where the regressed curve takes the unique maximal value of % Chl*a* (= 21.6) at Chl*a* of 0.67 [mg m^{-3}], which is also the maximum value over the entire Chl*a* range, while % Chl*a* in the in situ data fluctuates at the same Chl*a* value of 0.67 [mg m^{-3}]. Such a fluctuation of % Chl*a* at a given Chl*a* value would partly result from a temporal variation in phytoplankton community structure at a given geographical point, and partly from geographical spread of data points where the community composition is not necessarily the same. The mathematical representation within the ecological ambiguity is a limitation of the present approach. The data used to quantify the relationships, or to develop the algorithms, should ideally include sampling during pre- to post bloom periods for all ocean basins, providing a greater degree of confidence in the relationships. Continuous accumulation of in situ data to build such a data set would also enable a regular ongoing calibration of the relationships, improving detection of mid- and long-term variability in PFTs. Physiological changes in the phytoplankton due to environmental changes may be reflected by the regular calibration of the relationships over time.

4.3 Global distribution of PFTs

Figure 5 shows the global mean distributions of each PFT, derived from SeaWiFS Chl*a* observed over 1998–2009. Dinoflagellates are not considered here due to a poor result in the validation. Microplankton is relatively abundant at mid-high latitudes

BGD
7, 6675–6704, 2010

(Fig. 5a). Microplankton-dominated waters (i.e. % Chl*a* > 50%) are rather restricted along some parts of the Arctic and Antarctic coasts and coastal upwelling regions such as Benguela, Humbolt and Canary current regions, where Chl*a* is relatively high (Fig. 5i). Thus, microplankton, which is almost an entire reflection of the diatoms at a synoptic scale (Fig. 5d), do not show a basin scale dominance in the mean field. Nanoplankton are ubiquitously distributed, and constitute approximately 35–57 [% Chl*a*], but less in the subtropical gyres (Fig. 5b). The results obtained in this study are consistent with those of Liu et al. (2009) who found that prymesiophytes (haptophytes) dominate the Chl*a*-normalized phytoplankton stock in modern oceans. The subtropical gyres are largely dominated by picoplankton (% Chl*a* > 65%, Fig. 5c), mostly by prokaryotes (Fig. 5g) which includes *Prochlorococcus* sp. (Fig. 5h). The exception is the South Pacific gyre where pico-eukaryotes explain a significant portion of picoplankton (> 40 [% Chl*a*]) (Fig. 5f), which may be supported by the in situ data analysis of Ras et al. (2008) who postulate a possible significance of pico-sized flagellates (i.e. pico-eukaryotes) in the South Pacific Ocean, especially at the surface. On average over the 1998–2009 period, Microplankton, Nanoplankton and Picoplankton explain 9.2, 44.2 and 46.8 [% Chl*a*] of global Chl*a*, whereas diatoms, green algae, pico-eukaryotes, prokaryotes and *Prochlorococcus* sp. explain approximately 6.0, 13.1, 14.5, 32.3 and 21.5 [% Chl*a*], respectively.

Figure 6 shows the monthly time series of % Chl*a* of each PFT for 7 major oceans and the global ocean. For the Arctic Ocean (Southern Ocean), only data from July (January) are shown because of the maximum spatial coverage during summer at high latitudes (Fig. 6a and b). Microplankton and nanoplankton show a weak inter-annual variability in these high latitude oceans, but this may result from the aliasing due to the sub-sampling of the summer data. In the other oceans (Fig. 6c–h), the global relationships applied to satellite observation reproduce clear seasonality of PFTs, although a dynamic range (and an amplitude) of the temporal variability is subject to the populations in the continental shelf, which is not considered here due to a limitation of DPA. In the North Pacific (Fig. 6e), a secondary bloom, which is weaker than the primary

BGD
7, 6675–6704, 2010

spring bloom, is also visible in microplankton and diatoms. In all ocean basins (except the Arctic and Southern Ocean), microplankton and picoplankton are inversely correlated (recall Fig. 2). Nanoplankton also co-varies with them, but accompanying a phase difference. For example, nanoplankton is out of phase with picoplankton by a few months in the North Atlantic and North Pacific (Fig. 6c and e), whereas it is completely out of phase (approx. 6 months) in the South Pacific (Fig. 6f) and Indian Ocean (Fig. 6g).

Figure 6 also shows that the wide-spread distribution of nanoplankton with a relatively high spatial average value of % Chl*a* shown in Fig. 5b is maintained in the time series, implying that nanoplankton can be synoptically viewed as a background group in the total phytoplankton community. Although the mean % Chl*a* of picoplankton is also as high as that of nanoplankton over years, spatial distribution of picoplankton (Fig. 5c) is relatively limited to subtropical oceans, thus picoplankton is less ubiquitous than nanoplankton. Nonetheless, we note that picoplankton may also be viewed as background community when absolute Chl*a* (instead of % Chl*a*), and/or a particular basin such as subtropical gyres rather than the entire globe, are focused. Microplankton and diatoms have relatively sharp variation in time in comparison with nano- and picoplankton in North Atlantic and Pacific (Fig. 6c and e), implying intensive blooms in specific periods in a year. The dynamic range or amplitude of the bloom could be enhanced if continental shelves (white areas in Fig. 5), which are known as areas where a large microplankton blooms occur, were included in the analysis. Recalling that the spatial distributions of microplankton and diatoms are limited to some parts of midhigh latitude and coastal areas (Fig. 5a and d), microplankton and diatoms seem dominant only at a localized scale, both spatially and temporally, rather than as a background group in synoptic scale. However, a number of patches dominated by them, whether they are associated with turbulent flows such as eddies or not, could be found in the open oceans during a "snap shot" ship observation. Supporting the global view of microplankton and diatom distributions, Obayashi et al. (2001) also suggested that, in the subarctic North Pacific, a ubiquitous basic structure made up of diverse population

BGD
7, 6675–6704, 2010

is apparent, on which a flourishing diatom population, limited by area and season, is superimposed sporadically.

The spatial distribution and temporal variation of PFTs captured by SeaWiFS are based on the empirical relationships between Chl*a* and % Chl*a* obtained from in situ data taken at various time of the year in the global surface oceans. While the derived relationships reasonably reproduced the PFT structure within the time span of the data (1997–2008) as shown in (Fig. 4), an extrapolation of the relationships over the future satellite observation may introduce an ambiguity between natural fluctuations of the PFTs and a potential drift of the empirical relationships from reality. When the relationships are viewed as algorithms to estimate the PFTs, re-calibration of the algorithm may be required constantly over time to reduce the ambiguity. Such a calibration of the algorithm has been conducted several times over, for example, the SeaWiFS mission (the most recent re-calibration is 2009.1 reprocessing which we used in this work).

The results presented in this work are limited to the surface and synoptic applications. Caution must be taken when the relationships are applied to analysis for smaller scales, in space or time (i.e. within a narrower Chl*a* range), because an increased noise-to-signal ratio in the relationships is expected from Fig. 2: Fluctuations of % Chl*a* (or variability along y-axis in Fig. 2) at a fairly limited range of Chl*a* can become significantly large relative to variability of Chl*a* itself (or variability along x-axis), which may result in a degraded or less-defined relationship between Chl*a* and % Chl*a* for each PFTs. Furthermore, in coastal waters, although they were excluded in our analysis, the definition of biomarker pigments may be degraded due to an increased population of dinoflagellates, which can contain Fuco (Wright and Jeffrey, 2006) and confuses interpretation of the Fuco signal as a biomarker pigment of diatoms, requiring a further correction to Fuco.

The present approach uses only Chl*a* to derive % Chl*a* of the PFTs, although it was able to capture a dominant ecological feature of the global distribution of PFTs. Uitz et al. (2006) additionally uses mixed layer depths to take vertical structures of Chl*a*, hence PFTs, into account in order to better represent phytoplankton community. Although our

BGD
7, 6675–6704, 2010

focus was on the surface structure of PFTs, such multivariate approach using relevant quantities may reduce uncertainty in the estimation of PFTs.

Acknowledgements. Satellite ocean colour data (Sea-viewing Wide Field-of-view Sensor, SeaWiFS) were obtained from NASA Goddard Space Flight Centre. The authors also would like to appreciate NASA for, and all individuals and organisations contributed to, the SeaWiFS Bio-optical archive and Storage System (SeaBASS) and bio-Optical Marine Algorithm Dataset (NOMAD). This research is funded by National Centre for Earth Observation (NCEO) by Natural Environment Research Council (UK) and Global Climate Observation Mission (GCOM) by JAXA (Japan).

References

Aita, M. N., Yamanaka, Y., and Kishi, M.: Interdecadal variation of the lower trophic ecosystem in the northern Pacific between 1948 and 2002, in a 3-D implementation of the NEMURO model, Ecol. Model., 202, 81–94, 2007.

Aiken, J., Fishwick, J., Lavender, S., Barlow, R., Moore, G. F., Sessions, H., Bernard, S., Ras, J., and Hardman-Mountford, N.: Validation of MERIS reflectance and chlorophyll during the BENCAL cruise October 2002: preliminary validation of new demonstration products for phytoplankton functional types and photosynthetic parameters, Int. J. Remote Sens., 28, 497–516, 2007.

Aiken, J., Pradhan, Y., Barlow, R., Lavender, S., Poulton, A., Holligan, P., and Hardman-Mountford, N. J.: Phytoplankton pigments and functional types in the Atlantic Ocean: a decadal assessment, 1995–2005, Deep-Sea Res. Pt. II, 56, 899–917, 2009.

Allen, J., Aiken, J., Anderson, T. R., Buitenuis, E, Cornell, S., Geider, R. J., Haines, K., Hirata, T., Holt, J., LeQuéré, C., Hardman-Mountford, N. J., Ross, O. N., Sinha, B., and While, J.: Marine ecosystem models for earth systems applications: The MarQUEST experience, J. Mar. Syst., 81, 19–33, 2010.

Alvain, S., Moulin, C., Dandonneau, Y., and Breon, F. M.: Remote sensing of phytoplankton groups in case 1 waters from global SeaWiFS imagery, Deep-Sea Res. Pt. I, 1(52), 1989–2004, 2005.

BGD

7, 6675–6704, 2010

Alvain, S., Moulin, C., Dandonneau, Y., and Loisel, H.: Seasonal distribution and succession of dominant phytoplankton groups in the global ocean: A satellite view, Global Biogeochem. Cy., 22, GB3001, doi:10.1029/2007GB003154, 2008.

Barlow, R., Stuart, V., Lutz, V., Sessions, H., Sathyendranath, S., Platt, T., Kyewalyanga, M., Clementson, L., Fukasawa, M., Watanabe, S., and Devred, E.: Seasonal pigment patterns of surface phytoplankton in the subtropical southern hemisphere, Deep-Sea Res. Pt. I, 54, 1687–1703, 2007.

Behrenfeld, M. J. and Falkowski, P. G.: Photosynthetic rates derived from satellite-based chlorophyll concentration, Limnol. Oceanogr., 42, 1–20, 1997.

Blackford, J., Allen, J. I., and Gilbert, F.: Ecosystem dynamics at six contrasting sites: A generic modelling study, J. Mar. Syst., 52, 191–215, 2004

Behrenfeld, M. J., O'Malley, R. T., Siegel, D. A., McClain, C. R., Sarmiento, J. L., Feldman, G. C., Milligan, A. J., Falkowski, P. G., Letelier, R. M., and Boss, E. S.: Climate-driven trends in contemporary ocean productivity, Nature, 444, 752–755, doi:10.1029/2007GL031745, 2006.

Brewin, R. J. W., Sathyendranath, S., Hirata, T., Lavender, S., Baraciela, R. M., and Hardman-Mountford, N.: A three-component model of phytoplankton size class for the Atlantic ocean, Ecol. Model., 221(11), 1472–1483, 2010.

Devred, E., Sathyendranath, S., Studart, V., Maass, H., Ulloa, O., and Platt, T.: A two-component model of phytoplankton absorption in the open ocean: Theory and applications, J. Geophys. Res., 111, C03011, doi:10.1029/2005JC002880, 2006

Gregg, W. W., Ginoux, P., Schopf, P. S., and Casey, N. W.: Phytoplankton and iron: validation of a global three-dimensional ocean biogeochemical model, Deep-Sea Res. Pt. II, 50, 3143-3169, 2003

Gregg, W. W. and Casey, N. W.: Modeling coccolithophores in the global oceans, Deep-Sea Res. Pt. II, 54, 447–477, 2007.

Hashioka, T. and Yamanaka, Y.: Ecosystem change in western North Pacific associated with global warming using 3D-NEMURO, Ecol. Model., 202, 95–104, 2007.

Hirata, T., Aiken, J., Hardman-Mountford, N., Smyth, T. J., and Barlow, R.: An absorption model to determine phytoplankton size classes from satellite ocean colour, Remote Sens. Environ., 112, 3153–3159, 2008.

BGD

7, 6675–6704, 2010

Isada, T., Kuwata, A., Saito, H., Ono, T., Ishi, M., Yoshikawa-Inoue, H., and Suzuki, K.: Photosynthetic feastures and primary productivity of phytoplankton in the Oyashio and Kuroshio-Oyashio trasition regions of the northwest Pacific, J. Plankton Res., 31, 1009–1025, 2009.

Kishi, M. J., Kashiwai, M., Ware, D. M., Megrey, B. A., Eslinger, D. L., Werner, F. E., Noguchi-Aita, M., Azumaya, T., Fujii, M., Hashimoto, S., Huang, D., Iizumi, H., Ishida, Y., Kang, S., Kantakov, G. A., Kim, H., Komatsu, K., Navrotsky, V. V., Smith, S. L., Tadokoro, K., Tsuda, A., Yamamura, O., Yamanaka, Y., Yokouchi, K., Yoshie, N., Zhang, J., Zuenko, Y. I., and Zvalinsky, V. I.: NEMURO-a lower trophic level model for the North Pacific marine ecosystem, Ecol. Model., 202, 12–25, 2007.

Le Quéré, C., Harrison, S. P., Prentice, I. C., Buitenhuis, E. T., Aumont, O., Bopp, L., Claustre, H., Cotrim Da Cunha, L., Geider, R., Giraud, X., Klaas, C., Kohfeld, K. E., Legendre, L., Manizza, M., Platt, T., Rivkin, R. B., Sathyendranath, S., Uitz, J., Watson, A. J., and Wolf-Gladrow, D.: Ecosystem dynamics based on plankton functional types for global ocean biogeochemistry models, Global Change Biol., 11, 2016–2041, 2005.

Le Quéré, C. and Pesant, S.: Ecosystem dynamics based on plankton functional types for global ocean biogeochemistry models, EOS, Transactions, Am. Geophys. Union, 90, 30–31, 2009.

Liu, H., Probert, I., Uitz, J., Claustre, H., Aris-Brosou, S., Frada, M., Not, F., and de Vargas, C.: Extreme diversity of noncalcifying haptophytes explains a major pigment paradox in open oceans, P. Natl. Acad. Sci. USA, 106, 12803–12808, 2009.

Longhurst, A., Sathyendranath, S., Platt, T., and Caverhill, C.: An estimate of global primary production in the ocean from satellite radiometer data, J. Plankton Res., 17, 1245–1271, 1995.

Nair, A., Sathyendranath, S., Platt, T., Morales, J., Stuart, V., Forget, M. H., Devred, E., and Bouman, H.: Remote sensing of phytoplankton functional types, Remote Sens. Environ., 112, 3366–3375, 2008.

Obayashi, Y., Tanoue, E., Suzuki, K., Handa, N., Nojiri, Y., and Wong, C. S.: Spatial and temporal variabilities of phytoplankton community structure in the northern North Pacific as determined by phytoplankton pigments, Deep-Sea Res. Pt. I, 48, 439–469, 2001.

O'Reilly, J. E., Maritorena, S., Mitchell, B. G., Siegel, D. A., Carder, K. L., Garver, S. A., Kahru, M., and McClain, C.: Ocean color chlorophyll algorithm for SeaWiFS, J. Geophys. Res., 103(C11), 24937–24953, 1998.

BGD
7, 6675–6704, 2010

Polovina, J. J., Howell, E. A., and Abecassis, M.: Ocean's leaset productive waters are expanding, Geophys. Res. Lett., 35, L03618, doi:10.1029/2007GL031745, 2008.
Petihakis, G., Triantafyllou, G., Pollani, A., Koliou, A., and Theodorou, A.: Field data analysis and application of a complex water column biogeochemical model in different areas of a semi-enclosed basin: towards the development of an ecosystem management tool, Mar. Environ. Res., 59, 493–518, 2005
Ras, J., Claustre, H., and Uitz, J.: Spatial variability of phytoplankton pigment distributions in the Subtropical South Pacific Ocean: comparison between in situ and predicted data, Biogeosciences, 5, 353–369, doi:10.5194/bg-5-353-2008, 2008.
Raitsos, D. E., Lavender, S. J., Maravelias, C. D., Haralambous, J., Richardson, A. J., and Reid, P. C.: Identifying four phytoplankton functional types from space: An ecological approach, Limnol. Oceanogr., 53(2), 605–613, 2008.
Sathyendranath, S., Watts, L., Devred, E., Platt, T., Caverhill, C., and Maass, H.: Discrimination of diatoms from other phytoplankton using ocean-colour data, Mar. Ecol.-Prog. Ser., 272, 59–68, 2004.
Suzuki, K., Minami, C., Liu, H., and Saino, T.: Temporal and spatial pattern of chemotaxonomic algae pigments in the subarctic Pacific and the Bering Sea during the early summer of 1999, Deep-Sea Res. Pt. II, 49, 5685–5704, 2002.
Suzuki, K., Hinuma, A., Saito, H., Kiyosawa, H., Liu, H., Saino, T., and Tsuda, A.: Responses of phytoplankton and heterotrophic bacteria in the northwest subarctic Pacific to in situ iron fertilization as estimated by HPLC pigment analysis and flow cytometry, Prog. Oceanogr., 64, 167–187, 2005.
Tarran, G. A., Heywood, J. L., and Zubkov, M. V.: Latitudal changes in the standing stocks of nano- and picoeukaryotic phytoplankton in the Atlantic Ocean, Deep-Sea Res. Pt. II, 53, 1516–1529, 2006.
Uitz, J., Claustre, H., Morel, A., and Hooker, S. B.: Vertical distribution of phytoplankton communities in open ocean, An assessment based on surface chlorophyll, J. Geophys. Res., 111, C08005, doi:10:1029/2005JC003207, 2006
Vidussi, F., Claustre, H., Manca, B. B., Luchetta, A., and Marty, J.: Phytoplankton pigment distribution in relation to upper thermocline circulation in the eastern Mediterranean Sea during winter, J. Geophys. Res., 106(C9), 19939–19956, 2001.

BGD
7, 6675–6704, 2010

Werdell, P. J. and Bailey, S. W.: An improved in-situ bio-optical data set for ocean color algorithm development and satellite data product validation, Remote Sens. Environ., 98, 122–140, 2005.

Wright, S. W. and Jeffrey, S. W.: Pigment markers for phytoplankton production, Hdb. EnvIRON. Chem., Part N, 2, 71–104, 2006.

Zubkov, M. V., Sleigh, M. A., Tarran, G. A., Burkill, P. H., Leakey, R. J. G.: Picoplanktonic community structure on an Atlantic transect from 50 N to 50 S, Deep-Sea Res. Pt. I, 45, 1339–1355, 1998.

BGD

7, 6675–6704, 2010

Table 1. Diagnostic Pigments.

Size Classes/PFTs	Diagnostic Pigments	Estimation Formula
Microplankton	Fucoxanthin (Fuco), Peridinin (Perid)	1.41 (Fuco + Perid) / ΣDP[1]
/Diatoms	Fuco	1.41 Fuco/ΣDP[1]
/Dinoflagellates	Perid	1.41 Perid/ΣDP[1]
Nanoplankton	19′-Hexanoyloxyfucoxanthin (Hex)	(X_n × 1.27 Hex + 1.01 Chl*b* +0.35 But + 0.60 Allo)/ΣDP[2]
	Chlorophyll-*b* (Chl*b*)	
	Butanoyloxyfucoxanthin (But)	
	Alloxanthin (Allo)	
Picoplankton	Zeaxanthin (Zea), Hex, Chl*b*	(0.86 Zea + Y_p 1.27 Hex)/ΣDP[2]
/Prokaryotes	Zea	0.86 Zea/ΣDP[1]
/PicoEukaryotes	Hex, Chl*b*	
/*Prochlorococcus* sp.	Divinyl Chlorophyll-*a* (DVChl*a*)	0.86 DVChl*a*/Chl*a*
Green algae	Chl*b*	1.01 Chl*b*/ΣDP[1]

[1] ΣDP = 1.41 Fuco + 1.41 Perid + 1.27 Hex + 0.6 Allo + 0.35 But + 1.01 Chl*b* + 0.86 Zea = Chl*a* (Uitz et al., 2006)

[2] X_n indicates a proportion of nanoplankton contribution in Hex, respectively. Similarly Y_p indicates a proportion of picoplankton in Hex, respectively (Brewin et al., 2010)

BGD
7, 6675–6704, 2010

Table 2. Equations to estimate PFT fractions [0.0–1.0]. Set PFT fraction to 1.0 if > 1.0, and 0 if < 0. To get % Chl*a*, multiply 100 to the fractions derived.

SizeClass/PFTs	Formula	a_0	a_1	a_2	a_3	a_4	a_5	a_6
Micro	$\left[a_0 + \exp\,(a_1 x + a_2)\right]^{-1}$	0.7756	−2.4271	0.6031	–	–	–	–
/Diatoms	$\left[a_0 + \exp\,(a_1 x + a_2)\right]^{-1}$	1.3637	−3.2867	0.5013	–	–	–	–
/Dinoflagellates	(= Micro-diatoms)	–	–	–	–	–	–	–
Nano	(= 1-Micro-Pico)	–	–	–	–	–	–	–
/Green algae	$(a_0/y)\,\exp\left[a_1(x + a_2)^2\right]$	0.5379	−0.9623	−0.9982	–	–	–	–
Pico	$-\left[a_0 + \exp\,(a_1 x + a_2)\right]^{-1} + a_3 x + a_4$	0.1708	1.1453	−1.4202	−1.8037	2.7047	–	–
/Prokaryotes	$(a_0/a_1/y)\,\exp\left[a_2(x + a_3)^2/a_1^2\right]$ $+ a_4 x^2 + a_5 x + a_6$	0.0043	0.4915	−5.5052	0.9182	0.1144	−0.1062	0.0683
/Pico-Eukaryotes	(= Pico-Prokaryotes)	–	–	–	–	–	–	–
/Prochlorococcus sp.	$(a_0/a_1/y)\,\exp\left[a_3(x + a_4)^2/a_1^2\right]$ $+ a_4 x^2 + a_5 x + a_6$	0.0078	0.5564	−5.3204	0.95175	0.0136	−0.1650	0.0405

$x = \log_{10}(\text{Chl}a)$; $y = \text{Chl}a$

BGD
7, 6675–6704, 2010

Table 3. Statistical results of the reconstructed relationships between PFTs and Chl*a* against in situ data.*

Size Class/ PFT	Observed range of % Chl*a*	r^2	p	RMSE [%]	Max. Error [%]	Chl*a* at Max Error [mg m^3]
Microplankton	0–87	0.76	< 0.001	6.7	33.0	1.07
/Diatoms	0–84	0.72	< 0.001	6.6	34.7	1.07
/Dinoflagellates	0–40	0.19	< 0.001	2.3	27.4	2.14
Nanoplankton	7–72	0.66	< 0.001	7.5	21.6	0.33
/Green algae	0–40	0.56	< 0.001	4.6	21.3	1.45
Picoplankton	6–90	0.79	<0.001	6.6	26.4	1.45
/Prokaryotes	1—72	0.76	< 0.001	7.1	25.5	0.14
/Pico-Eukaryotes	2–40	0.42	< 0.001	4.9	20.9	1.45
/Prochlorococcus sp.	0–55	0.76	< 0.001	6.1	20.1	0.11
Mean		0.62	<0.001	5.8	25.6	1.02

* Rounded values

BGD
7, 6675–6704, 2010

Table 4. Validation results.*

Size Class/PFT	slope	intercept	r^2	p	RMSE [%]
Microplankton	1.130	−0.024	0.742	< 0.001	7.52
/Diatoms	1.228	−0.333	0.743	< 0.001	7.46
/Dinoflagellates	0.311	2.396	0.089	0.080	1.78
Nanoplankon	1.168	−7.980	0.661	< 0.001	7.52
/Green algae	0.782	2.636	0.483	< 0.001	4.36
Picoplankton	1.103	−5.593	0.835	< 0.001	6.42
/Prokaryotes	1.011	−0.699	0.752	< 0.001	7.33
/Pico-Eukaryotes	0.734	4.007	0.330	< 0.001	4.84
/Prochlorococcus sp.	1.111	−1.479	0.770	< 0.001	6.68
Mean	0.951	−0.785	0.601	<0.001	5.99

* Rounded values

BGD
7, 6675–6704, 2010

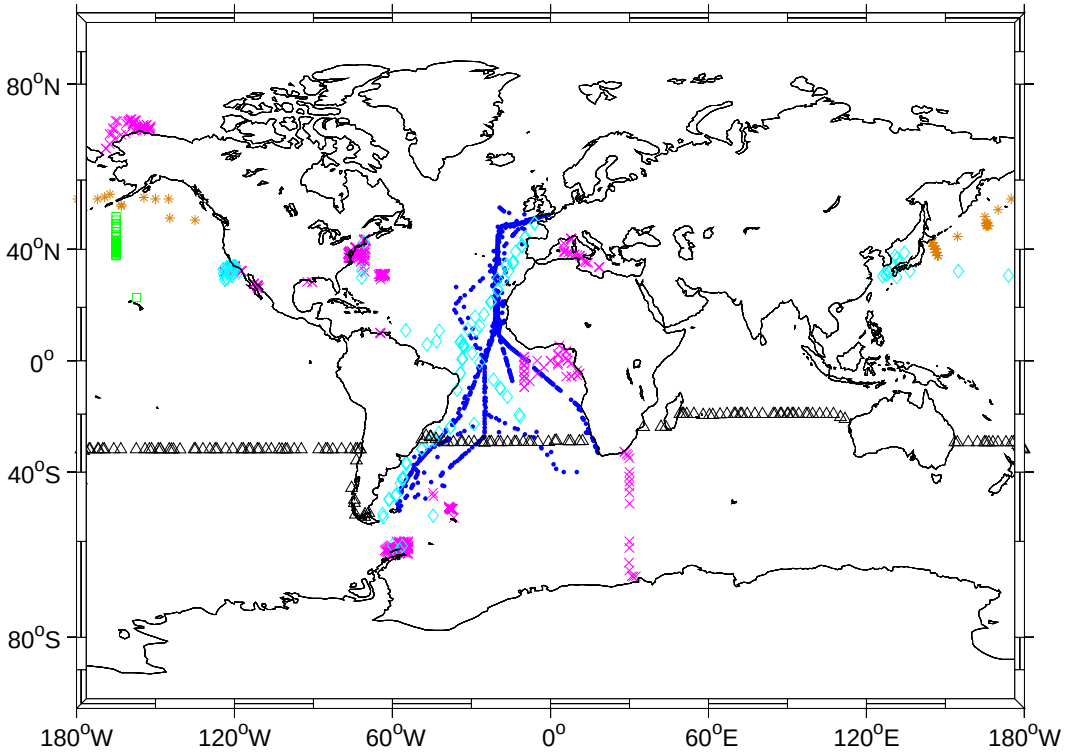

Fig. 1. Distribution of phytoplankton pigment data used in this study; blue filled diamond: the NERC AMT cruise (Aiken et al., 2009), black triangle: the JAMSTEC BEAGLE cruise (Barlow et al., 2007), cyan open diamond: the NASA NOMAD (Werdell and Bailey, 2005), magenda cross: the NASA SeaBASS, blue star: the SEEDS II cruise (Suzuki et al., 2005) + A-line stations (Isada et al., 2009), green open square: the HU Oshoro-maru cruise.

BGD
7, 6675–6704, 2010

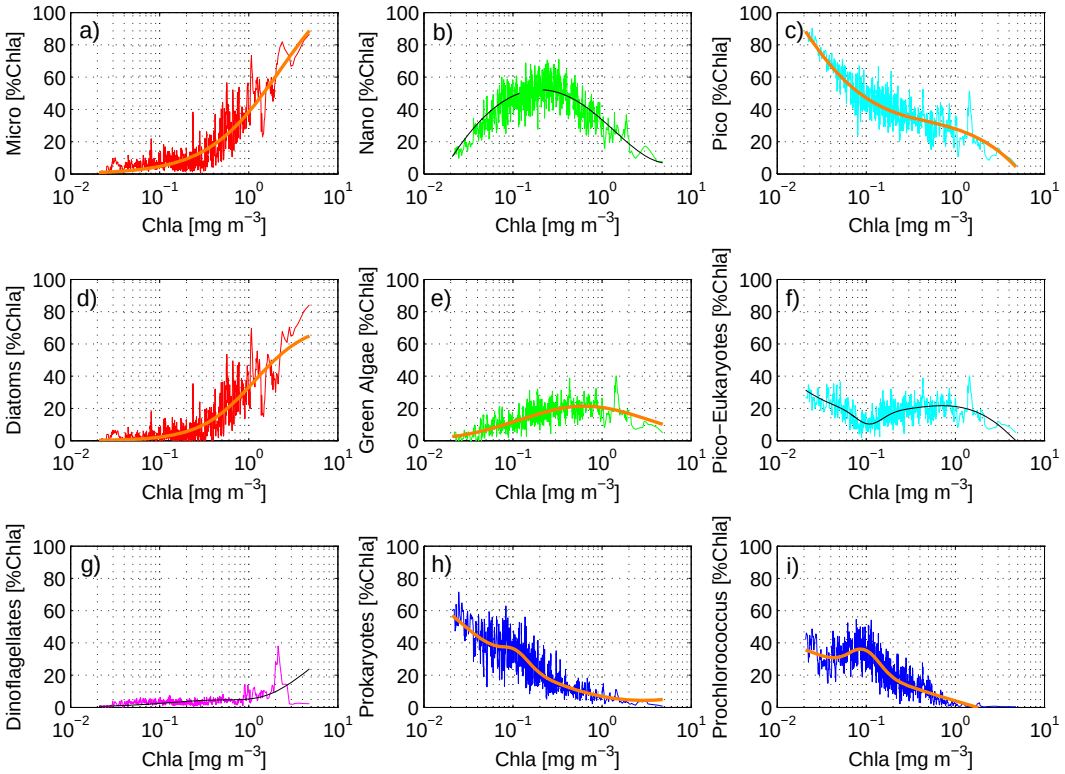

Fig. 2. Global relationships between Chl*a* and % Chl*a* of each PFT; **(a)** Microplankton, **(b)** Nanoplankton, **(c)** Picoplankton, **(d)** Diatoms, **(e)** Green algae, **(f)** Pico-Eukaryotes, **(g)** Prokaryotes, **(h)** *Prochlorococcus* sp. The orange thick curves are the least-square fits to the original data (a, c, d, e, h, i), whereas the black thin curves are the fits indirectly derived from the least square fits (b, f, g; e.g. Nano = 100% – $\text{Micro}_{\text{fit}}$ – Pico_{fit}, see Table 2).

BGD
7, 6675–6704, 2010

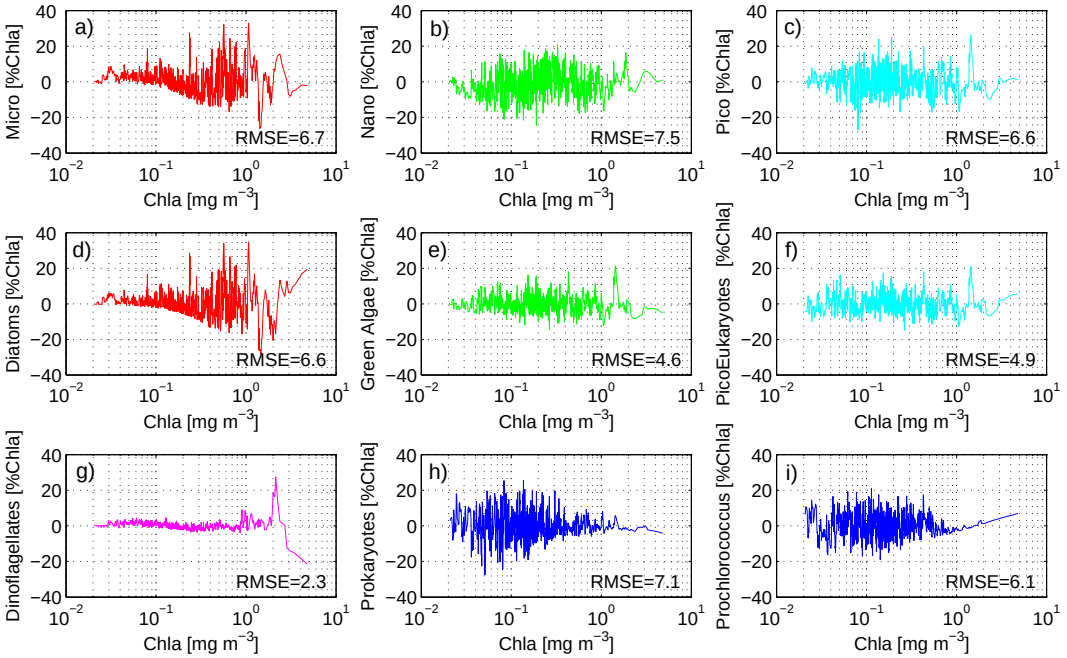

Fig. 3. Uncertainties of the synoptic relationships between Chl*a* and %Chl*a* of each PFT; **(a)** Microplankton, **(b)** Nanoplankton, **(c)** Picoplankton, **(d)** Diatoms, **(e)** Green Algae, **(f)** Pico-Eukaryotes, **(g)** Prokaryotes, **(h)** *Prochlorococcus* sp.

BGD
7, 6675–6704, 2010

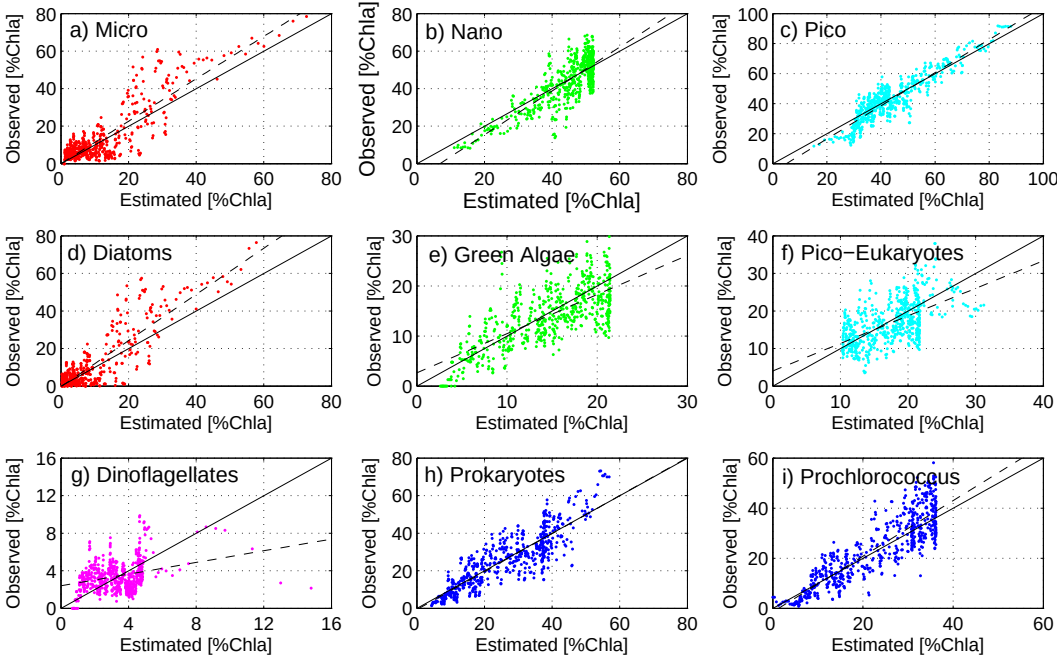

Fig. 4. Results of validation. **(a)** Microplankton, **(b)** Nanoplankton, **(c)** Picoplankton, **(d)** Diatoms, **(e)** Green Algae, **(f)** Pico-Eukaryotes, **(g)** Dinoflagellates, **(h)** Prokaryotes, **(i)** *Prochlorococcus* sp.

BGD
7, 6675–6704, 2010

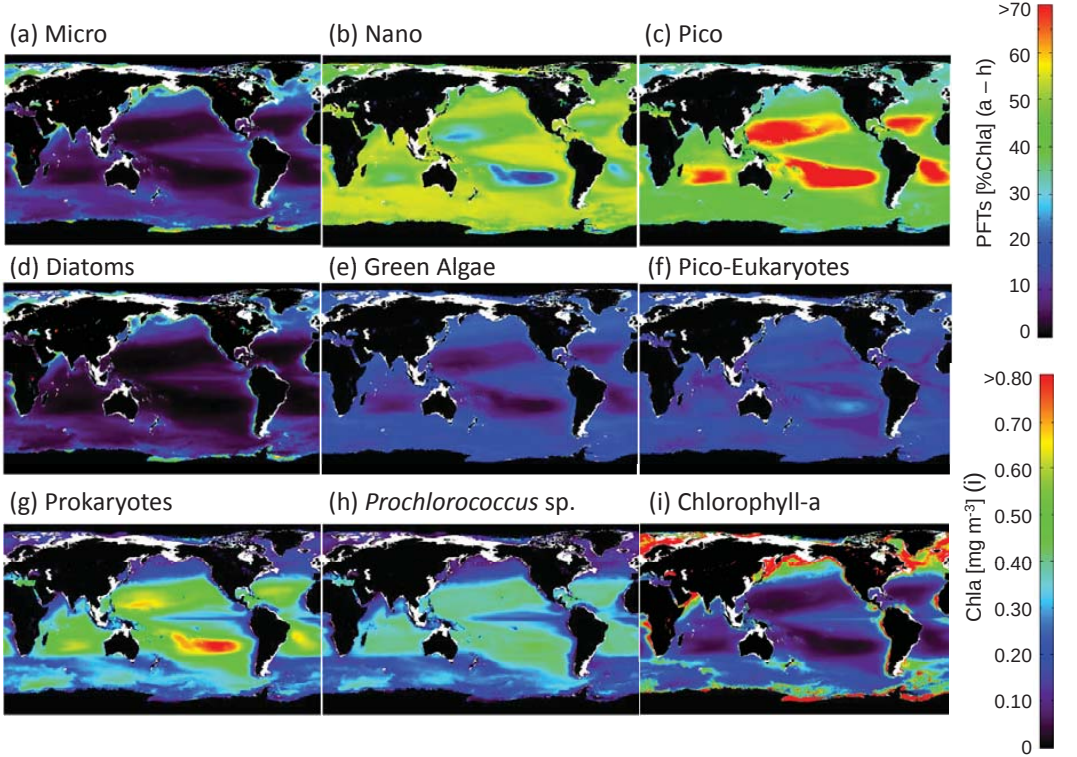

Fig. 5. Synoptic distribution of surface PFTs [% Chl*a*] and Chl*a* [mg m^{-3}] over 1998–2009 derived from SeaWiFS. **(a)** Microplankton, **(b)** Nanoplankton, **(c)** Picoplankton, **(d)** Diatoms, **(e)** Green Algae, **(f)** Pico-Eukaryotes, **(g)** Prokaryotes, **(h)** *Prochlorococcus* sp., **(i)** Chlorophyll-*a*. White area shows a continental shelf mask defined by < 200 m

BGD
7, 6675–6704, 2010

Relationships between Chlorophyll-*a* and diagnostic pigments

T. Hirata et al.

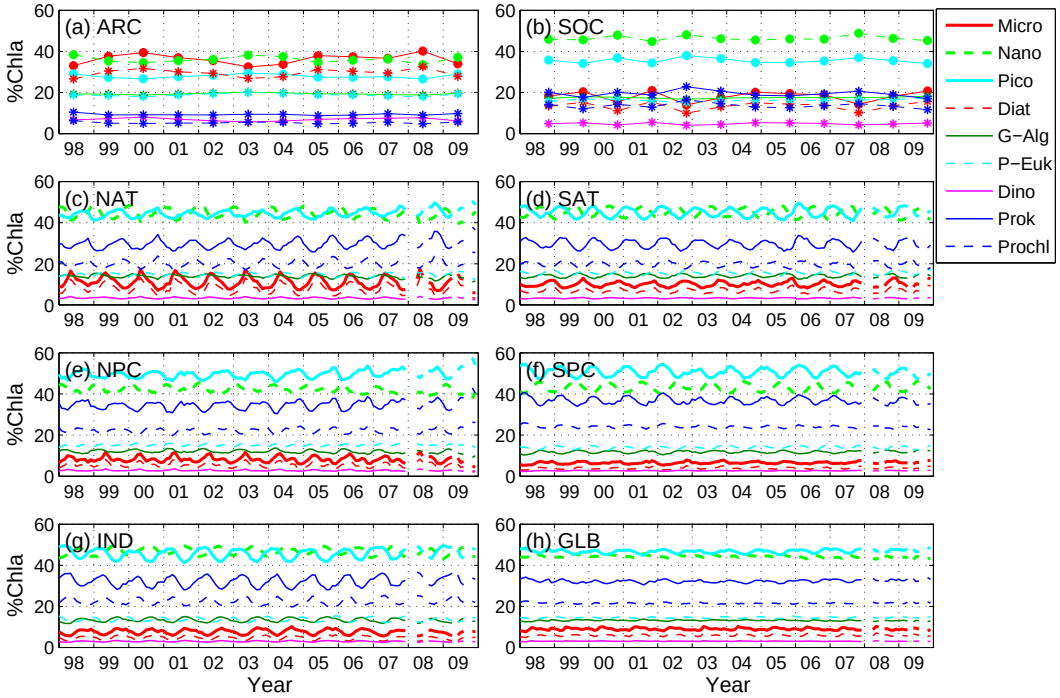

Fig. 6. 12-year time series (1998–2009) of % Chl*a* of each PFT derived from SeaWiFS satellite chla; **(a)** Arctic Oceans; **(b)** Southern Ocean; **(c)** North Atlantic; **(d)** South Atlantic; **(e)** North Pacific; **(f)** South Pacific; **(g)** Indian Ocean; **(h)** Global Oceans. For the Arctic and Southern Oceans, only June and Jan data are plotted to represent summer data since they give the maximum geographical coverage in the regions and the satellite Chl*a* is not available for winter period. There are missing data in January to March and July in 2008 as well as May, September and October in 2009 due to technical troubles on SeaWiFS.

BGD
7, 6675–6704, 2010